IEEE Access
Multidisciplinary | Rapid Review | Open Access Journal

Received January 3, 2019, accepted January 31, 2019, date of publication February 13, 2019, date of current version April 2, 2019.

Digital Object Identifier 10.1109/ACCESS.2019.2898881

Gas Sensor Array Dynamic Measurement Uncertainty Evaluation and Optimization Algorithm

WENWEN ZHANG[1], LEI WANG[1,2], LIHUA YE[1,3], PEILONG LI[1], AND MINGXUE HU[2]

[1]College of Electronics and Information Engineering, Tongji University, Shanghai 201804, China
[2]College of Sino-German, Tongji University, Shanghai 201804, China
[3]Department of Mathematical and Information Engineering, Jiaxing University, Jiaxing 314001, China

Corresponding author: Wenwen Zhang (zhangwenwen_1203@163.com)

This work was supported in part by the National Key R&D Program of China under Grant 2017YFE0100900.

ABSTRACT Metal oxide semiconductor (MOS) gas sensor array dynamic measurement uncertainty evaluation, which currently mainly uses static measurement approximation estimations, cannot accurately distinguish the measured value of the sudden change of the measured value caused by the dynamic mutation of the measured gas or the actual sensor array local fault caused by the sudden change of the measured value, thereby resulting in a dynamic measurement process of the MOS gas sensor array uncertainty evaluation results and the validation measurement value reliability being greatly reduced. This paper presents a dynamic adaptive Kalman filter andGray bootstrap comprehensive modified prediction model for the dynamic measurement uncertainty evaluation. The dynamic adaptive Kalman filter and Gray bootstrap method is used to estimate the good performance of the probability distribution function of the measured value, and the uncertainty evaluation of the dynamic measurement state of the MOS gas sensor array is realized. Using the correlation of the dynamic adaptive Kalman filter and Gray model multisensor output, a new MOS gas sensor array measurement value confirmation algorithm is proposed to distinguish the measured value mutation caused by the normal dynamic mutation of the measured gas and the fault of the real sensor array. Finally, the MOS gas sensor array measurement is set up, and the experiments show that the proposed MOS gas sensor array dynamic measurement uncertainty evaluation and an optimization algorithm is effective.

INDEX TERMS Sensor array, dynamic measurement, uncertainty, dynamic adaptive Kalman filter.

I. INTRODUCTION

The uncertainty in sensor array measurement is the main indicator of the quality of the sensor evaluation measurement, which is used to characterize the dispersion of the measured value [1]–[3]. Currently, the domestic evaluation of sensor dynamic measurement uncertainty is still in its infancy and a complete fundamental theoretical system has not been formed.

The International Measurement Uncertainty Research Committee proposed that GUM (Guide to the Expression of Uncertainty in Measurement) is only suitable for static measurement conditions. In real-life measurement systems, the dynamic uncertainty is often evaluated. In the case of less demanding measurements, the static measurement uncertainty estimation is often used instead of the dynamic measurement uncertainty estimation. In an MOS gas sensor array system, the static approximation substitution method has a large error compared with the real uncertainty estimation.

The paper in [4] and [5] proposed a new strategy for using polynomial prediction filters and validating the random fuzzy variables (VRFV) for online measurement verification and verification uncertainty (VU) estimation of multifunctional self-verification sensors, but they lack a comprehensive performance comparison with other common prediction algorithms. The paper in [6] considered a wavelet analysis, aimed at measuring the synthesis of transient disturbances and provides a general expression that affects the uncertainty of the synthesis. Simulations have been performed to verify the correctness of the above expressions, but the scheme

The associate editor coordinating the review of this manuscript and approving it for publication was Syed Mohammad Zafaruddin.

regarding the uncertainty in Wavelet-Based signal analysis is not suitable for gas sensor array dynamic measurement uncertainty evaluation. The paper in [7] proposed a sensor error detection, isolation and recovery strategy, proposing a GM (1,1) (Gray Model) Gray Bootstrap model for sensor array uncertainty evaluation. The feasibility of the proposed sensor array dynamic measurement uncertainty evaluation model is verified, but there is a large error between the model and the actual dynamic measurement uncertainty evaluation. The scheme does not consider the impact of sensor array failure or the sudden change of the measured gas.

In the papers in [4], [5], and [8], a functional framework of a multifunctional self-verification sensor was proposed. Aimed at the influence of a sudden failure of the sensor on the evaluation of uncertainty, a functional scheme of the FDIR strategy for a predictive filter was proposed. The sensor output value is compared with the actual sensor output. The absolute value of the difference is then compared with the set safety threshold to correct the sensor measurement value. This paper provides a feasible solution for the sensor dynamic measurement to distinguish sensor faults, but does not provide a solution for the uncertainty assessment of the sensor array dynamic measurement. The paper in [9] and [10] presented a novel dictionary learning method to improve the gas identification performance of electronic noise. They are simpler, but they also lead to very competitive classification results. This method is not only effective in signal analysis but also useful for enhancing the performance of the current electronic noises. However, the article does not assess the dynamic measurement uncertainty of the proposed measurement scheme. The paper in [11]–[14] designed a low-power, handheld gas sensor array with temperature sensitivity and cross-sensitivity for industrial applications. It can accurately measure such gases as O_2, CO, CH_4 and H_2S. Additionally, a surface fitting algorithm was proposed to reduce the influence of the cross-sensitivity and improve the measurement accuracy by one to two orders of magnitude. This paper solved the gas sensor cross-sensitivity problem, but did not propose a reasonable solution to the uncertainty measurement of the entire measurement dynamic system. The paper in [15]–[18] compiled an authoritative review of works published on measurement uncertainty since 2004 and described the measurement uncertainty evaluation scheme. However, there are few papers on the dynamic uncertainty of sensor arrays. In the papers in [19]–[21], the uncertainty of the generalized Lambda distribution of expressions is described, but the proposed algorithm is not suitable for the estimation of measurement uncertainty of MOS gas sensor arrays. The paper in [18], [22], and [23] discussed the uncertainty assessment in indirect measurements, where the main concern is the measurement model. Its input is modeled as a dependent random variable, but this method has a large error in evaluating the dynamic uncertainty of the MOS gas sensor array and the calculation process is complicated. In the paper in [7], Shen et al. proposed a traditional GUM self-confirmed multisensor uncertainty evaluation method in 2012. This method mainly analyzes various uncertainty sources and derives the uncertainty of the MRVM data reconstruction model. The transfer function finally uses the static measurement uncertainty GUM uncertainty synthesis formula to obtain the dynamic sensor measurement uncertainty. This method solves the evaluation problem of dynamic measurement uncertainty, but the scheme still results in a large error.

Due to the time-varying nature, complexity and uncertainty of dynamic measurement systems, traditional prediction models (such as autoregressive moving average models and nonlinear regression models) are not suitable for dynamic measurement systems. In this paper, a dynamic uncertainty evaluation method based on a dynamic, adaptive Kalman filter-Gray Bootstrap method is proposed. The dynamic performance of the MOS gas sensor array is achieved by the dynamic adaptive Kalman filter-Gray self-help method to estimate the performance of the measured value probability distribution function. With an uncertainty evaluation under the measurement state and using the dynamic adaptive Kalman filter-Gray model to predict the value under the dynamic measurement state, an XOR (exclusive or) MOS gas sensor array measurement value confirmation algorithm is proposed to accurately distinguish the normal dynamics of the measured gas. Mutations and sudden changes in the measured values are caused by faulty sensor arrays.

The model is based on Kalman filtering, Gray theory, robust estimation, data fusion and variance component estimation. It mainly uses Kalman filtering to effectively estimate the observations with noise and combines the Gray prediction model to establish accurate values in small samples and poor information states. Using the robust estimation theory, data fusion technology and the variance component estimation theory to construct a dynamic adaptive Kalman filter-Gray comprehensive correction prediction model, the prediction of the MOS gas sensor array becomes more accurate. The main contributions of this paper are as follows:

(1) This paper presents a dynamic adaptive Kalman filter-Gray bootstrap comprehensive modified prediction model, where the advantages of Kalman filter theory in estimating the observed values with noise are utilized. Combined with the advantages of the Gray prediction model in establishing the prediction model under the condition of poor information, the dynamic adaptive Kalman filter-Gray synthesis is constructed by using robust estimation theory, data fusion technology and variance component estimation theory. Combined with the modified prediction model, the sensor array can more accurately predict the gas in a dynamic environment.

(2) In this paper, a dynamic adaptive Kalman filter-Gray prediction model is proposed. Based on the correlation of the multi sensor output, an XOR MOS gas sensor array measurement value confirmation algorithm is proposed to accurately distinguish the measured value of the mutation caused by the normal dynamic change of the measured gas and the real sensor array obstacle. This further solves the problem of confirming the decrease in the accuracy of the measured value due to the failure of the MOS gas sensor array.

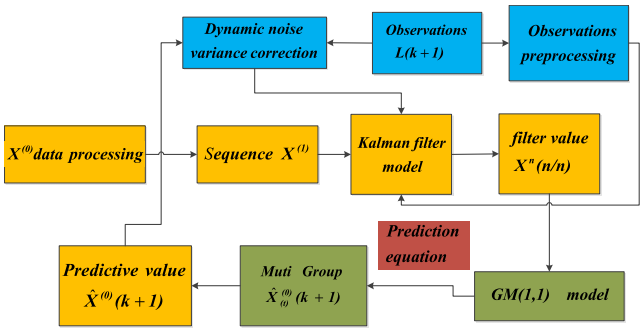

FIGURE 1. Dynamic adaptive Kalman filter-Gray prediction model.

II. DYNAMIC ADAPTIVE KALMAN FILTER-GRAY BOOTSTRAP COMPREHENSIVE MODIFIED PREDICTION MODEL

The Gray system theory was proposed by Professor Deng Julong from the Huazhong University of Science and Technology and applied to the Gray system, where "some information is known and some information is unknown". In this paper, based on Kalman filter theory, Gray theory, robust estimation, data fusion and variance component estimation, a dynamic adaptive Kalman filter-Gray prediction model is established. This model mainly combines the advantages of Gray prediction to achieve prediction in a poor information state and Kalman filtering theory to effectively estimate the observations containing noise, and then combines these with a robust estimation theory. The flow chart of the dynamic adaptive Kalman filter-Gray prediction model in this paper is given in Figure 1.

The 4 steps of a dynamic adaptive Kalman filter-Gray bootstrap comprehensive modified prediction model implementation process are given below:

The first step is GM (1,1) Modeling Based on Kalman Filter.

1. Sensor array detection data accumulation processing.

It is assumed that for the indoor space to be tested, a number n of the MOS gas sensor sampling arrays are distributed. In the dynamic measuring system, the gas sensor obtains the original time series, expressed as in formula (1):

$$\boldsymbol{X} = \{x(1), x(2), \cdots, x(k), \cdots, x(n)\} \tag{1}$$

X(n): the measured value corresponding to the nth sampling point.

Then, the measured values obtained by the MOS gas sensors at the initial time are expressed as $\boldsymbol{X}^{(0)}$:

$$\boldsymbol{X}^{(0)} = \{x^{(0)}(1), x^{(0)}(2), \cdots, x^{(0)}(n)\}, \quad n \geq 2 \tag{2}$$

A first-order Accumulation Generation Operation (1-AGO) is performed on the data sequence detected by the MOS gas sensor $\boldsymbol{X}^{(0)}$, and a first-order accumulation generation sequence $\boldsymbol{X}^{(1)}$ is obtained:

$$\boldsymbol{X}^{(1)} = \{x^{(1)}(1), x^{(2)}(2), \cdots, x^{(1)}(n)\} \tag{3}$$

$$x^{(1)}(k) = \sum_{i=1}^{k} x^{(0)}(i), \quad k = 1, 2, \cdots n \tag{4}$$

The AGO processing of the sensor measurement data sequence is important, as it enables the deterministic information contained in the original data sequence to be monotonically grown and enhanced by AGO processing. It can also partially cancel random noise.

2. Calculating the filtered value of the accumulated sequence

The following is done to obtain the filtered value of the accumulated sequence. The filtering is derived from the control field while the measured value with error is processed to obtain the desired estimated value. In fact, many measurement errors are generated during the measurement process of the MOS gas sensor array. Transforming the above equation (2) into equation (3), the Kalman filter model can then be established.

$$\boldsymbol{X}(k/k) = \boldsymbol{X}(k/k-1) + \boldsymbol{J}_k[\boldsymbol{L}_k - \boldsymbol{B}_k\boldsymbol{X}(k/k-1)]\boldsymbol{\Omega}_k \tag{5}$$

$$\boldsymbol{D}_x(k/k) = (\boldsymbol{E} - \boldsymbol{J}_k\boldsymbol{B}_k)\boldsymbol{D}_k(k/k-1) \tag{6}$$

$$\boldsymbol{X}(k/k-1) = \boldsymbol{\Phi}_{k,k-1}\boldsymbol{X}(k-1/k-1) \tag{7}$$

$$\begin{aligned}\boldsymbol{D}_x(k/k-1) = {} & \boldsymbol{\Phi}_{k,k-1}\boldsymbol{D}_x(k-1/k-1)\boldsymbol{\Phi}^T_{k,k-1} \\ & + \boldsymbol{\Gamma}_{k,k-1}\boldsymbol{D}_\Omega(k-1)\boldsymbol{\Gamma}^T_{k,k-1}\end{aligned} \tag{8}$$

$$\begin{aligned}\boldsymbol{J}_k = {} & \boldsymbol{D}_x(k/k-1)\boldsymbol{B}^T_k[\boldsymbol{B}_k\boldsymbol{D}_x(k/k-1)\boldsymbol{B}^T_k \\ & + \boldsymbol{D}_\Delta(k)]^{-1}\end{aligned} \tag{9}$$

$\boldsymbol{X}(k/k)$: the time n-dimensional state vector;

$\boldsymbol{L}_k$: t_k momenta m-dimensional observation vector;

$\boldsymbol{D}_\Omega(k-1)$: t_k time r-dimensional dynamic noise variance;

$\boldsymbol{D}_\Delta(k)$: t_k M-dimensional observation noise at the moment;

$\boldsymbol{\Phi}_{k/k-1}$: $n \times n$ Dimension state transition matrix from time t_{k-1} to time t_k;

$\boldsymbol{\Omega}_k$: t_k dynamic noise matrix ($n \times r$);

$\boldsymbol{J}_k$: filter gain matrix;

The filtering model established by equation (5) is as follows:

$$\boldsymbol{X}^{(1)} = (\boldsymbol{X}^{(1)}(1/1), \boldsymbol{X}^{(1)}(2/2), \cdots, \boldsymbol{X}^{(1)}(n/n)) \tag{10}$$

3. Filter value subtraction processing

The filter model obtained above is subjected to subtraction processing to reduce it to a data sequence:

$$\boldsymbol{X}^{(0)} = (\boldsymbol{X}^{(0)}(1), \boldsymbol{X}^{(0)}(2), \cdots, \boldsymbol{X}^{(0)}(n)), \quad n \geq 2 \tag{11}$$

The above equation (11) is not the original sequence (2). The GM (1,1) model is established by using the abovementioned cumulative sequence, which is known from equation (4):

$$\boldsymbol{X}^{(1)}(k/k) = \sum_{i=1}^{k} \boldsymbol{X}^{(0)}(i), \quad k = 1, 2, \cdots n \tag{12}$$

4. Establishing the GM (1,1) model by using the reduced sequence

The dynamic GM (1,1) model is established using equation (10) as follows:

$$\frac{d\boldsymbol{X}^{(1)}(k/k)}{dt} + a(k)\boldsymbol{X}^{(1)}(k/k) = b(k) \tag{13}$$

The above equation discretizes the model as:

$$\boldsymbol{X}^{(0)}(k) = -a(k)\boldsymbol{X}^{(1)}(k/k) + b(k) \quad k = 2, 3\cdots n \tag{14}$$

$a(k)$ and $b(k)$ in the above equation (14) are taken as the dynamic parameters to be estimated. The response function of the differential equation (14) above can be expressed as:

$$\hat{\boldsymbol{X}}(k) = \{\int_0^k b(s)e^{\int_0^k a(r)dr}ds + c\}e^{-\int_0^k a(r)dr} \tag{15}$$

In the above equation (15), $b(s)$ and $a(r)$ are to be estimated.

where c is a constant, and $\hat{\boldsymbol{X}}(k)$ is the predicted value of $\boldsymbol{X}(k)$. The following uses the least squares method to find the parameters $a(k)$ and $b(k)$. Assuming Equation (16) to be the minimum:

$$s = \sum_{k=2}^{n}[-a(k)x^{(1)}(k/k) + b(k) - x^{(0)}(k)]^2 \tag{16}$$

set $a(k)$ and $b(k)$ be continuous functions and then we approximate with a polynomial of an appropriate number of terms. Setting A and B to have the following polynomial:

$$\begin{cases} a(k) = a_0 + a_1k + a_2k + \cdots a_pk^p \\ b(k) = b_0 + b_1k + b_2k^2 + \cdots b_qk^q \end{cases} \tag{17}$$

The undetermined coefficients in the above equation are:

$a_k(k = 0, 1, \cdots, p)$, and $b_l(l = 0, 1, \cdots q)$ We set equation (18):

$$s = \sum_{k=2}^{n}[-a(k)x^{(1)}(k/k) + b(k) - x^{(0)}(k)]^2 \tag{18}$$

the minimum undetermined coefficient of equation (18) satisfies the equation set (19):

$$\begin{cases} \dfrac{\partial s}{\partial a_k} = 0 \\ \dfrac{\partial s}{\partial b_l} = 0 \quad k = 0, 1, \cdots, p, l = 0, 1, \cdots q \end{cases} \tag{19}$$

i.e.:

$$\sum_{k=2}^{n}[(-\sum_{i=0}^{p}a_ik^iX^{(1)}(k/k) + \sum_{i=0}^{q}b_ik^i) - \boldsymbol{X}^{(0)}(k)](-k^k\boldsymbol{X}^{(1)}(k/k)) = 0 \tag{20}$$

Assuming (21)–(23), as shown at the bottom of the next page:

The observation equations can be listed according to equation (24):

$$\boldsymbol{Y} = \boldsymbol{B}\beta \tag{24}$$

Equation (24) is estimated according to the robust least squares parameter:

$$\boldsymbol{Y} = (\boldsymbol{B}^T\bar{\boldsymbol{P}}B)^{-1}\boldsymbol{B}^T\bar{\boldsymbol{P}}Y \tag{25}$$

The parameters $a_k(k = 0, 1, \cdots, p)$ and $b_l(l = 0, 1, \cdots q)$ can be calculated by determining parameters $a(k)$ and $b(k)$.

Then, we can calculate the predicted value $\hat{x}(k+1)$, and the integral complex trapezoidal formula can obtain $\hat{x}(k+1)$ in a discrete form as in formula (26):

$$\hat{x}^{(1)}(k+1/k+1) = \{\sum_{t=1}^{k}(\sum_{i=0}^{q}\hat{u}_it^i)e^{\sum_{i=0}^{p}\frac{\hat{a}_it^{i+1}}{i+1}} + c\}e^{-\sum_{i=0}^{p}\frac{\hat{a}_ik^{i+1}}{i+1}} \tag{26}$$

In the above formula $c = x^{(0)}(1)$ is the final subtraction and can obtain the predicted value $\hat{x}^{(0)}(k+1)$.

The second step is accuracy assessment and residual correction

5. Assessment of internal coincidence accuracy

To evaluate the aforementioned internal accuracy, the GM (1,1) model established by formula (10):

$$\frac{d\boldsymbol{X}^{(1)}(k/k)}{dt} + a(k)\boldsymbol{X}^{(1)}(k/k) = b(k) \tag{27}$$

Obtaining the model simulation value sequence:

$$\boldsymbol{X}_M^{(1)} = (\boldsymbol{X}_M^{(1)}(1/1), \boldsymbol{X}_M^{(1)}(2/2), \cdots X_M^{(1)}(n/n)) \tag{28}$$

The original data sequence is obtained using a transformation of equation (28):

$$\boldsymbol{X} = (X^{(0)}(1), X^{(0)}(2), \cdots X^{(0)}(n)), \quad n \geq 2 \tag{29}$$

And finding the model simulation sequence value:

$$\boldsymbol{X}_M^{(0)} = (\boldsymbol{X}_M^{(0)}(1/1), \boldsymbol{X}_M^{(0)}(2/2), \cdots \boldsymbol{X}_M^{(0)}(n/n)) \tag{30}$$

Thus, the residual sequence can be obtained:

$$\boldsymbol{\delta}_M^{(0)} = (\delta_M^{(0)}(1), \delta_M^{(0)}(2), \cdots, \delta_M^{(0)}(n)), \quad n \geq 2 \tag{31}$$

therefore:

$$\boldsymbol{\delta}_M^{(0)}(t) = \boldsymbol{X}^{(0)}(t) - \boldsymbol{X}_M^{(0)}(t) \tag{32}$$

Relative error expression:

$$\delta = \frac{\boldsymbol{\delta}_M^{(0)}(t)}{\boldsymbol{X}^{(0)}(t)} \times 100\% \tag{33}$$

The original MOS gas sensor array measurement is set to obtain $\boldsymbol{X}^{(0)}$ and the corresponding residual series as s_1^2 and s_2^2, respectively. The corresponding expressions of the calculation are as follows:

$$s_1^2 = \frac{1}{n}\sum_{k=1}^{n}(\boldsymbol{X}^{(0)}(k) - \bar{\boldsymbol{X}}^{(0)})^2 \tag{34}$$

$$s_2^2 = \frac{1}{n}\sum_{k=1}^{n}(\delta_M^{(0)}(k) - \bar{\delta}_M^{(0)}) \tag{35}$$

TABLE 1. Post-test difference ratio test standard.

Model accuracy level	P	C
Level 1 (good)	0.95-1	<0.35
Level 2(qualified)	0.8-0.95	0.35-0.5
Level 3 (barely)	0.7-0.8	0.5-0.65
Level 4(unqualified)	<0.7	>0.65

The average calculation formula is:

$$\bar{X}^{(0)}(k) = \frac{1}{n}\sum_{k=1}^{n} X^{(0)}(k) \tag{36}$$

$$\bar{\delta}_M^{(0)} = \frac{1}{n}\sum_{k=1}^{n} \delta_M^{(0)}(k) \tag{37}$$

The final calculation for the posterior difference ratio:

$$C = \frac{s_2}{s_1} \tag{38}$$

The small error probability calculation expression is as follows:

$$P = P\{|\delta_M^{(0)}(k) - \bar{\delta}_M^{(0)}| < 0.6745 s_1\} \tag{39}$$

The two most important indexes of the posterior margin ratio test are the posterior error ratio $\boldsymbol{C}$ and the small error ratio $\boldsymbol{P}$, in which the smaller the index $\boldsymbol{C}$ is the better, whereas the larger the index $\boldsymbol{P}$ is the better. The specific indicator standards are shown in Table 1:

6. Residual correction

The residual sequence GM (1,1) model is established using the residual sequence (31) obtained above:

The first order cumulative generating sequence expression for $\delta_M^{(1)}$ to $\delta_M^{(0)}$is as follows:

$$\boldsymbol{\delta}_M^{(1)} = (\delta_M^{(1)}(1), \delta_M^{(1)}(2), \cdots \delta_M^{(1)}(n)) \tag{40}$$

$$\boldsymbol{\delta}_M^{(1)}(k) = \sum_{i=1}^{k} \delta_M^{(0)}(i), \quad k = 1, 2, \cdots n \tag{41}$$

and set the matrix $\boldsymbol{Z}_\delta^{(1)}$ to be the immediate mean generation sequence of $\boldsymbol{\delta}_M^{(1)}$:

$$\boldsymbol{Z}_\delta^{(1)} = (z^{(1)}(2), z^{(1)}(3), \cdots, z^{(1)}(n)) \tag{42}$$

among them:

$$\boldsymbol{Z}_\delta^{(1)}(k) = 0.5(\delta_M^{(1)}(k) + \delta_M^{(1)}(k-1))(k = 2, 3, \cdots n) \tag{43}$$

Set $\hat{\boldsymbol{A}} = [a, b]^T$ to the parameter column and:

$$\boldsymbol{Y} = [\delta_M^{(0)}(2), \delta_M^{(0)}(3), \cdots, \delta_M^{(0)}(n)]^T \tag{44}$$

$$\boldsymbol{B} = \begin{bmatrix} -z^{(1)}(2) & -z^{(1)}(3) & \cdots & -z^{(1)}(n) \\ 1 & 1 & \cdots & 1 \end{bmatrix} \tag{45}$$

Obtain the GM (1,1) model:

$$\boldsymbol{\delta}_M^{(0)}(k) + az^{(1)}(k) = b \tag{46}$$

The least squares parameter column of the above GM (1,1) satisfies the following equation:

$$\hat{\boldsymbol{A}} = (\boldsymbol{B}^T\boldsymbol{B})^{-1}\boldsymbol{B}^T\boldsymbol{Y} \tag{47}$$

then the albino equation of the GM (1,1) model established by the above residual sequence:

$$\frac{d\boldsymbol{\delta}_M^{(1)}}{dt} + a\boldsymbol{\delta}_M^{(1)} = b \tag{48}$$

and the time response function is obtained from the above albino equation as:

$$\delta_M^1(t) = (\delta_M^{(1)}(1) - \frac{b}{a})e^{-at} + \frac{b}{a} \tag{49}$$

The GM (1,1) model is obtained from the above equation as: $\delta_M^{(0)}(k) + az^{(1)}(k) = b$, and the time corresponding sequence expression is:

$$\delta_M^{(1)}(k+1) = (\delta_M^{(1)}(1) - \frac{b}{a})e^{-at} + \frac{b}{a}, \quad k = 1, 2, \cdots n \tag{50}$$

setting $\gamma = \frac{b}{1+0.5a}$ and $\theta = \frac{a}{1+0.5a}$, the restore value is:

$$\boldsymbol{\delta}_M^{(0)}(k) = (\gamma - \theta\delta_M^{(0)}(1))e^{-a(k-2)} \tag{51}$$

The third step is the predicted value data fusion.

The following is a data fusion of the predicted values of the data detected by the MOS sensor. The accumulated data sequence is:

$$\boldsymbol{X}^{(1)} = (X^{(1)}(1/1), X^{(2)}(2/2), \cdots, X^{(1)}(n/n),$$

$$\boldsymbol{X}^{(1)}(k/k) = \sum_{i=1}^{k} X^{(0)}(i), \quad k = 1, 2, \cdots n \tag{52}$$

The model is different when selecting the different elements in the above data sequence $\boldsymbol{X}^{(1)}$ to establish the following equation (53):

$$\frac{d\boldsymbol{X}^{(1)}(k/k)}{dt} + a(k)X^{(1)}(k/k) = b(k) \tag{53}$$

$$\boldsymbol{\beta} = (a_0, a_1, \cdots, a_p, b_0, b_1, \cdots b_q)^T \tag{21}$$

$$\boldsymbol{Y} = (X^{(0)}(2), X^{(0)}(3), \cdots, X^{(0)}(n)) \tag{22}$$

$$\boldsymbol{B} = \begin{bmatrix} -X^{(1)}(2/2) & -2X^{(1)}(2/2) & \cdots & -2X^{(1)}(2/2) & 1 & 2 & \cdots & 2^q \\ -X^{(1)}(3/3) & -3X^{(1)}(3/3) & \cdots & -3X^{(1)}(3/3) & 1 & 3 & \cdots & 3^q \\ \vdots & \vdots & \cdots & \vdots & \vdots & \vdots & \vdots & \vdots \\ -X^{(1)}(n/n) & -nX^{(1)}(n/n) & \cdots & -nX^{(1)}(n/n) & 1 & n & \cdots & n^q \end{bmatrix} \tag{23}$$

We describe how to choose the following data sequence to build a Gray model:

$$(X^{(1)}(m-1/m-1), X^{(1)}(m/m), \cdots, X^{(1)}(n/n))m<n \quad (54)$$

This paper uses a selection of unequal dimensional data sequences:

$$\boldsymbol{X}_{(t)}^{(1)} = (X^{(1)}(m-1/m-1), X^{(1)}(m/m), \cdots, X^{(1)}(n/n)) \quad (55)$$

The above equation can be used to establish the model of equation (56).

Through equation (56) the equation models can be established, and the t prediction values can be simultaneously obtained:

$$\frac{dX^{(1)}(k/k)}{dt} + a(k)X^{(1)}(k/k) = b(k) \quad (56)$$

t: number of selected modeling data sequence; m-n+1: dimension of the selected data sequence. This article will use data fusion to solve for the best value.

Set the two predicted values to be the distance values between $\hat{X}_{(i)}^{0}(k+1)$ and $\hat{X}_{(j)}^{0}(k+1)$, respectively, as follows:

$$d_{ij} = |\hat{\boldsymbol{X}}_i^{(0)}(k+1) - \hat{X}_j^{(0)}(k+1)|, i, j \in \{1, 2, \cdots t\} \quad (57)$$

The support function r_{ij} between the two data must meet the following two conditions:

(1) r_{ij} is inversely proportional to the relative distance; that is, the greater the difference between the two values, the smaller the degree of support between them.

(2) $r_{ij} \in [0, 1]$; therefore, the advantages of the membership function in fuzzy set theory can be utilized to avoid the absolute degree of mutual support.

The support matrix functions established in this paper are as follows:

$$M = \begin{bmatrix} e^{-d_{11}} & e^{-d_{12}} & \cdots & e^{-d_{1m}} \\ e^{-d_{11}} & e^{-d_{11}} & \cdots & e^{-d_{2m}} \\ \vdots & \vdots & \vdots & \vdots \\ e^{-d_{m1}} & e^{-d_{m2}} & \cdots & e^{-d_{mm}} \end{bmatrix} \quad (58)$$

$$\boldsymbol{M} = (r_{ij})_{m\times m} \quad (59)$$

from $\hat{X}_{(t)}^{(0)}(k+1)$ to $\hat{X}^{(0)}(k+1)$, it is necessary to determine the weight ratio ω_i of $\hat{X}_{(t)}^{(0)}(k+1)$ and satisfy:

$$\sum_{i=1}^{m} \omega_i = 1 \quad (60)$$

In addition, the above ω_i comprehensively includes information between $r_{i1}, r_{i2}, \cdots r_{im}$, so that a group of nonnegative groups $v_1, v_2, \cdots, v_n$ can be determined, which satisfies:

$$\omega_i = \sum_{j=1}^{m} v_j r_{ij} \quad (61)$$

The matrix expression of the function is:

$$\boldsymbol{H} = \boldsymbol{MN} \quad (62)$$

$\boldsymbol{H}$: Represents a column vector consisting of ω_i; $\boldsymbol{N}$: Represents a column vector consisting of v_j; $\boldsymbol{M}$: Nonnegative symmetric matrix; there is a maximum modulus eigenvalue, and its corresponding eigenvector is $\boldsymbol{N}_\lambda = [v_1^\lambda, v_2^\lambda, \cdots, v_m^\lambda]$. The component is nonnegative and can be taken as:

$$\omega_i = \frac{v_i^\lambda}{\sum_{j=1}^{m} v_j^\lambda} \quad (63)$$

After fusion, the predicted values are:

$$\hat{X}^{(0)}(k+1) = \sum_{i=1}^{m} \omega_i \hat{X}_{(t)}^{(0)}(k+1) \quad (64)$$

Residual calculation:

$$q(k+1) = X^{(0)}(k+1) - \hat{X}^{(0)}(k+1) \quad (65)$$

Relative error calculation:

$$\delta = \frac{q(k+1)}{X^{(0)}(k+1)} \times 100\% \quad (66)$$

This paper requires $\delta < 10\%$.

The fourth step is dynamic noise variance correction

7. Adaptive Kalman filtering based on variance component estimation

A dynamic variance correction is performed below. Adaptive Kalman filtering based on the principle of variance component estimation is an adaptive filtering algorithm based on the dynamic residual variance component of the prediction residual calculation model. The Kalman filter equation is rewritten into a Gauss-Markov model, and taking the one-step predicted value $\hat{X}^0(k+1)$ as a pseudo-observation value, the covariance matrix is $\boldsymbol{D}(\hat{X}^0(\mathrm{k}+1))$, and the observation equation:

$$\boldsymbol{L}_k = \boldsymbol{B}_k \boldsymbol{X}_k + \Delta_k \quad (67)$$

The above is rewritten into an equation $\boldsymbol{V} = \boldsymbol{A}\boldsymbol{X}^0(k) - \boldsymbol{L}$

The weight matrix of error equation $\boldsymbol{P}$ is as follows:

$$\boldsymbol{V} = \begin{bmatrix} V_{\hat{X}^0(k+1)} \\ V_{L_k} \end{bmatrix} \quad \boldsymbol{A} = \begin{bmatrix} \boldsymbol{E} \\ \boldsymbol{B} \end{bmatrix}$$
$$\boldsymbol{L} = \begin{bmatrix} \hat{X}^0(k+1) \\ L_k \end{bmatrix} \quad \boldsymbol{P} = \begin{bmatrix} D^{-1} & 0 \\ 0 & D_{\Delta_k}^0 \end{bmatrix} \quad (68)$$

The above equation contains pseudo observations and actual observations. In the following, based on the principle of postestimation, the expression of the preresidual is assumed to be:

$$\boldsymbol{V}_k = B_k \hat{X}^0(k+1) - L_k \quad (69)$$

the variance of $L_k, \hat{X}^0(k+1)$ is:

$$\boldsymbol{D}(L_k) = \boldsymbol{\delta}_{L_0}^2 \boldsymbol{P}_{L_k}^{-1} \quad (70)$$

$$\boldsymbol{D}(\hat{\boldsymbol{X}}^0(k+1)) = \boldsymbol{\delta}_{x_0}^2 \boldsymbol{P}_{\hat{X}^0(k+1)}^{-1} \quad (71)$$

The above equation assumes that $\delta_{L_0}^2$ and $\delta_{x_0}^2$ are all equal to 1. Then, the variance of the residual is predicted:

$$\begin{aligned} \boldsymbol{D}(V_k) &= \boldsymbol{B}_k \boldsymbol{D}(\hat{\boldsymbol{X}}^0(k+1))\boldsymbol{B}_k^T + \boldsymbol{D}(L_k) \\ &= \delta_{x_0}^2 \boldsymbol{B}_k P_{\hat{x}^0(k+1)}^{-1} \boldsymbol{B}_k^T + \delta_{L_0}^2 + \boldsymbol{P}_{L_k}^{-1} \end{aligned} \tag{72}$$

Through adjustment, the following is calculated:

$$\begin{aligned} \boldsymbol{E}(\boldsymbol{V}_k^T \boldsymbol{P}_{L_k} \boldsymbol{V}_k) &= tr(\boldsymbol{P}_{L_k} \boldsymbol{D}(\boldsymbol{V}_k)) \\ &= \mathrm{tr}(\boldsymbol{P}_{L_k}(\delta_{x_0}^2 \boldsymbol{B}_k \boldsymbol{P}_{\hat{x}^0(k+1)}^{-1} \boldsymbol{B}_k^T) + \delta_{L_0}^2 \boldsymbol{P}_{L_k}^{-1})) \\ &= \delta_{x_0}^2 tr(\boldsymbol{P}_{L_k} \boldsymbol{B}_k \boldsymbol{P}_{\hat{x}^0(k+1)}^{-1} \boldsymbol{B}_k^T) + \delta_{L_0}^2 m \end{aligned} \tag{73}$$

where m is the number of observations.

If the variance of the actual observation value L is taken as a known value, the variance component $\delta_{x_0}^2$ estimate of the pseudo observation value can be solved according to the above equation:

$$\delta_{x_0}^2 = \frac{\boldsymbol{E}(\boldsymbol{V}_k^T \boldsymbol{P}_{L_k} \boldsymbol{V}_k) - \delta_{L_0}^2 m}{tr(\boldsymbol{P}_{L_k} \boldsymbol{B}_k \boldsymbol{P}_{\hat{X}^0(k+1)}^{-1} \boldsymbol{B}_k^T)} \tag{74}$$

$\boldsymbol{D}(\hat{X}^0(k+1))$ can be represented as two parts as follows, and the dynamic noise variance component is represented by $\delta_{\Omega_0}^2$:

$$\begin{aligned} &\boldsymbol{D}(\hat{\boldsymbol{X}}^0(k+1)) \\ &= \delta_{x_0}^2 \boldsymbol{P}_{\hat{X}^0(k+1)}^{-1} \\ &= \delta_{X_0}^2 (\boldsymbol{\Phi}_{k,k} \boldsymbol{D}_{\hat{X}^0(k+1)} \boldsymbol{\Phi}_{k,k-1}^T + \boldsymbol{\Gamma}_{k,k-1} \boldsymbol{D}_{\Omega_{k-1}} \boldsymbol{\Gamma}_{k,k-1}^T \\ &= \delta_{X_0}^2 \boldsymbol{\Phi}_{k,k-1} \boldsymbol{D}_{\hat{X}^0(k+1)} \boldsymbol{\Phi}_{k,k-1}^T + \delta_{\Omega_0}^2 \boldsymbol{\Gamma}_{k,k-1} \boldsymbol{D}_{\Omega_{k-1}} \boldsymbol{\Gamma}_{k,k-1}^T \end{aligned} \tag{75}$$

using the above equations with $\delta_{L_0}^2$ and $\delta_{x_0}^2$ as known values, the estimated value of the dynamic noise variance component $\delta_{\Omega_0}^2$ is solved:

$$\begin{aligned} \boldsymbol{\delta}_{\boldsymbol{\Omega_0}}^{\boldsymbol{2}} &= [\boldsymbol{E}(\boldsymbol{V}_{\boldsymbol{k}}^{\boldsymbol{T}} \boldsymbol{P}_{\boldsymbol{L_k}} \boldsymbol{V}_{\boldsymbol{k}})] \\ &\quad - \boldsymbol{\delta}_{\boldsymbol{x_0}}^{\boldsymbol{2}} \boldsymbol{tr}(\boldsymbol{P}_{\boldsymbol{L_k}} \boldsymbol{B_k} \boldsymbol{\Phi}_{\boldsymbol{k,k-1}} \boldsymbol{D}_{\hat{\boldsymbol{x}}^{\boldsymbol{0}}(\boldsymbol{k+1})} \boldsymbol{\Phi}_{\boldsymbol{k,k-1}}^{\boldsymbol{T}} \boldsymbol{B}_{\boldsymbol{k}}^{\boldsymbol{T}}) \\ &\quad - \boldsymbol{\delta}_{\boldsymbol{L_0}}^{\boldsymbol{2}} \boldsymbol{m}] / \boldsymbol{tr}(\boldsymbol{P}_{\boldsymbol{L_k}} \boldsymbol{B_k} \boldsymbol{\Gamma}_{\boldsymbol{k,k-1}} \boldsymbol{D}_{\boldsymbol{\Omega_{k-1}}} \boldsymbol{\Gamma}_{\boldsymbol{k,k-1}}^{\boldsymbol{T}} \boldsymbol{B}_{\boldsymbol{k}}^{\boldsymbol{T}}) \end{aligned} \tag{76}$$

By using the abovementioned prediction residual, the variance observation a priori value is known, and the variance component of the predicted value is estimated by the above steps. The dynamic noise variance component is estimated, which can effectively overcome the filter's instability.

8. Variance Compensation Adaptive Filtering

Variance compensation adaptive filtering is applied. Assuming that $\boldsymbol{V}_k$ is the prediction residual between the measured value and the final predicted value, the variance matrix D_w of $\boldsymbol{V}_k$ is:

$$\begin{aligned} \boldsymbol{D}_w = &\boldsymbol{B}_{k+i} \boldsymbol{\Phi}_{k+i,k} \boldsymbol{D}_{X_k} \boldsymbol{\Phi}_{k+i,k}^T \boldsymbol{B}_{k+i}^T + \boldsymbol{D}_{\Delta_{k+i}\Delta_{k+i}} \\ &+ \sum_{\gamma=k+i}^{k+i} \boldsymbol{B}_{k+i} \boldsymbol{\Phi}_{k+i} \boldsymbol{\Gamma}_{\gamma,\gamma-1} \boldsymbol{D}_{\Omega_{\gamma-1}\Omega_{\gamma-1}} \boldsymbol{\Phi}_{k+i,\gamma}^T \boldsymbol{B}_{k+i}^T \end{aligned} \tag{77}$$

$$\boldsymbol{B}_{k+i} \boldsymbol{\Phi}_{k+i,k} \boldsymbol{\Gamma}_{\gamma,\gamma-1} = \boldsymbol{A}^{(k+i,\gamma)} = [a_{hj}^{(k+i,\gamma)}] \tag{78}$$

In the above equation $r = 1, \cdots, N \quad k = 1, \cdots, n$, assume that $\boldsymbol{D}_{\Omega_{\gamma-1}\Omega_{\gamma-1}}$ is a constant diagonal matrix over the observation period $t_{k+1}, t_{k+2}, \cdots, t_{k+N}$, i.e., the expression is as follows:

$$\boldsymbol{D}_{\Omega_{\gamma-1}\Omega_{\gamma-1}} = \begin{bmatrix} \delta_{11}^2 & \cdots & \cdots & 0 \\ 0 & \delta_{22}^2 & \cdots & 0 \\ \vdots & \vdots & \vdots & \vdots \\ 0 & \cdots & \cdots & \sigma_{\gamma\gamma}^2 \end{bmatrix} = \boldsymbol{D}_{\Omega\Omega} \tag{79}$$

$$diag\boldsymbol{D}_{\Omega\Omega} = (\delta_{11}^2, \delta_{22}^2, \cdots, \delta_{rr}^2)^T \tag{80}$$

according to:

$$\boldsymbol{E}(\boldsymbol{V}_{k+i}^T \bullet \boldsymbol{V}_{k+i}) = tr[\boldsymbol{E}(\boldsymbol{V}_{k+i} \bullet \boldsymbol{V}_{k+i}^T)] = tr\boldsymbol{D}_w \tag{81}$$

$$V_{k+i}^T \bullet V_{k+i} = trD_w + \eta_{k+i} \tag{82}$$

η_{k+i} : Zero mean white noise sequence, $r = 1, \cdots, N$

$$\begin{aligned} \boldsymbol{E}_{k+i} = &\boldsymbol{V}_{k+i}^T \bullet \boldsymbol{V}_{k+i} - tr[\boldsymbol{B}_{k+i} \boldsymbol{\Phi}_{k+i} \boldsymbol{D}_{X_k} \boldsymbol{\Phi}_{k+i,k}^T \boldsymbol{B}_{k+i}^T] \\ &- tr\boldsymbol{D}_{\Delta_{k+i}\Delta_{k+i}} \end{aligned} \tag{83}$$

$$\boldsymbol{E} = [E_{k+i}, \cdots, E_{k+N}]^T \tag{84}$$

$$\boldsymbol{\eta} = [\eta_{k+i}, \cdots, \eta_{k+N}]^T \tag{85}$$

then:

$$\boldsymbol{E} = A\mathrm{diag}\boldsymbol{D}_{\Omega\Omega} + \eta \tag{86}$$

For the linear equations of the above equation for $\boldsymbol{D}_{\Omega\Omega}$, when $N \geq r$ there is a unique solution, and the LS of $\mathrm{diag}\boldsymbol{D}_{\Omega\Omega}$ is estimated to find $\boldsymbol{D}_{\Omega\Omega}$ over any period of time as a real-time estimate of the dynamic noise covariance.

This paper first preprocesses the data detection of the MOS gas sensor array, then accumulates the sequence of settlement observation data to generate time series $\boldsymbol{X}^{(1)}$. It then constructs the Kalman filter model by the $\boldsymbol{X}^{(1)}$ sequence, then obtains the filter value $\boldsymbol{X}^{(n)}(n/n)$ of $\boldsymbol{X}^{(1)}$ sequence through Kalman filter to reduce the sequence:

$$X^{(0)}(k+1) = X^{(1)}(k+1/k+1) - X^{(1)}(k+1) \tag{87}$$

The GM (1,1) model is established, and the parameters are obtained by the robust estimation method. The internal matching accuracy is evaluated according to the established model GM (1,1), and the residual correction model is established for the sequence $\boldsymbol{\delta}_M^{(0)}$ to correct the prediction model. According to the prediction equations for data sequences of different step sizes, multiple sets of predicted values $\boldsymbol{X}_{(t)}^0(k+1)$ are obtained, and the final predicted result $\hat{\boldsymbol{X}}^{(0)}(k+1)$ is obtained by data fusion. Finally, the final prediction result $\hat{\boldsymbol{X}}^{(0)}(k+1)$ is used to obtain the prediction residual based on the observed value $\boldsymbol{L}_{k+1}$. The variance component is estimated based on the residual and the dynamic noise estimation value $\delta_{\Omega_0}^2$ is obtained. In this way, the dynamic noise variance correction makes the filter equation continuously change in order to overcome the instability of the filter.

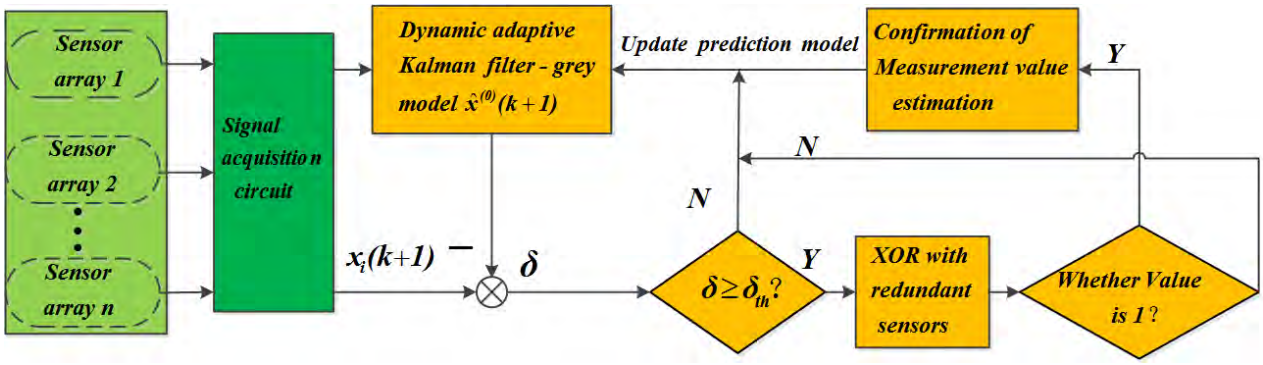

FIGURE 2. Block diagram of the measuring value of the MOS gas sensor array.

III. XOR MOS GAS SENSOR ARRAY MEASUREMENT VALUE VALIDATION ALGORITHM

The measurement accuracy of the MOS gas sensor array directly affects the qualitative analysis of the gas, which leads to the failure of the entire detection and control system. To solve the above problems, this paper proposes a method for confirming the measured value based on an XOR MOS gas sensor array. It is able to correctly identify the sudden change of the measured gas, faults in the self-gas sensor array and prevent failed sensor arrays from affecting subsequent inspection and analysis results.

The block diagram of the measured value from the XOR MOS gas sensor array proposed in this paper is shown in Fig. 2.

With redundant MOS gas sensor arrays, all sensors can independently represent the trend of the measured gas, and the responses of all gas sensor arrays remain consistent with the sudden change of the measured gas. The steps for confirming the measured value based on the XOR MOS gas sensor array are as follows:

(1) Gas time series detected by all redundant MOS gas sensor arrays:

$$\boldsymbol{X} = \{x(1), x(2), \cdots, x(k), \cdots, x(n)\} \tag{88}$$

establishing their respective dynamic adaptive Kalman filter-Gray models.

(2) By using the above dynamic adaptive Kalman filter-Gray model to obtain the final predicted value $x_i^{(0)}(k+1)$, the error term δ_i between the detected value $x_i(k+1)$ of the real sensor array and the predicted value $x_i^{(0)}(k+1)$ can be obtained. The error threshold δ_{th} and the threshold value ($\delta_{th} = 4\delta_i$) are set. Once the predicted error value $|\delta_i|$ is greater than the set error threshold δ_{th}, the sensor measurement value is abrupted, and the output signal truth table is set. The truth table is shown in Table 2:

(3) The XOR outputs at 1 sensor array and the redundant sensor array. If the output is logic 1, it indicates that the sensor array has a fault. If the output is logic 0, the detected gas has a sudden change. The above fault description truth table is shown in Table 3:

TABLE 2. Output signal truth table.

Comparative Val	Output Val $f(x_i(k))$
$\delta_i < 4\delta_{th}$	0
$\delta_i \geq 4 \mid \delta_{th} \mid$	1

TABLE 3. XOR fault truth table.

XOR Value $g(x_i(k))$	Output Val
1	The sensor array failed
0	The gas to be tested is abrupt

When the MOS gas sensor array signal is abrupted by a sudden change in the gas to be tested, the dynamic adaptive Kalman filter-Gray model needs to be updated online to ensure the prediction accuracy in the entire dynamic process; when the MOS gas sensor array fails, the fault value is replaced with the predicted measured value, and then the adaptive Kalman filter-Gray model is updated.

The MOS gas sensor measurement value confirmation algorithm is given below. The algorithm is as shown in the following Algorithm 1:

The MOS gas sensor measurement value confirmation algorithm proposed in this paper can determine the cause for the abrupt signal change in the dynamic detection process of the MOS gas sensor. If the MOS gas sensor array fails and interferes at sample point $k+1$, the measured value $x_i(k+1)$ will be replaced by $\hat{x}_i(k+1)$. The measured value sequence will also be rewritten as $X_i^{new} = \{x_i(2), x_i(3), \cdots, \hat{x}_i(k+1)\}$ to update the dynamic adaptive Kalman filter-Gray model to reduce the impact of sensor failure on its confirmed measurement and dynamic measurement uncertainty evaluation results.

IV. UNCERTAINTY EVALUATION ALGORITHM IN A DYNAMIC MEASUREMENT STATE

In the machine olfactory system, the quality of the MOS gas sensor array detection measurement directly affects the accuracy of gas detection. The accuracy of the measured

Algorithm 1 Fault Detection and Confirmation for Sensor Arrays

Input: The measured data sequence $\boldsymbol{X}(i)$of each sensor in the sensor array.
Output: MOS sensor measurement value confirmation result
1: Initialize the parameters of the Dynamic adaptive Kalman filter-Gray model.
2: Build the Dynamic adaptive Kalman filter-Gray model for each sensor.
3**: for** each sensor measured data sequence$x(k+1)$ do
4: Predict the current measured value $\hat{x}_i(k+1)$ by Dynamic adaptive Kalman filter-Gray model
5: Calculate difference $|\delta_i|$ between the measured data value $x_i(k+1)$and the predicted measured data value $\hat{x}_i(k+1)$
6: **if**$_{|\delta_i|<\delta_{th}}$ **then**
7: No change in measured value, $f(x_i(k+1))=0$
8: **else**
Mutation of measured value, $f(x_i(k+1))=1$
With redundant gas sensor array XOR detection
9: **end if**
10**: if** $g(x_i(k+1))=0$ **then**
The measured value of sensor i is normal
11: **end if**
12: **if** $g(x_i(k+1))=1$ **then**
The measured value of sensor i is abnormal
13:**end if**
14: **end for**

values needs to be evaluated before the measured values are used. The measurement uncertainty is an important indicator for evaluating the quality of the measured values. Aimed at the characteristics of the dynamic measurement system of the MOS gas sensor array, in this paper we propose an uncertain evaluation algorithm based on the dynamic adaptive Kalman filter-Gray bootstrap method, which is based on the uncertainty method of dynamic self-measurement in the Gray bootstrap method.

(1) Detecting the original measured value sequence for the MOS gas sensor array mentioned above:

$$\boldsymbol{X}^{(0)}=\{x^{(0)}(1),x^{(0)}(2),\cdots,x^{(0)}(n)\},\quad n\geq 2 \tag{89}$$

Using the Bootstrap in statistics to perform a resampling of $\boldsymbol{X}^{(0)}$ by k times to obtain a new sequence $\boldsymbol{X}_b^{(0)}$;

(2) Repeat the above step (1) B times to obtain an equal possible resampling self-matrix:

$$\boldsymbol{X}_{bootstrap}=(\boldsymbol{X}_1^{(0)},\boldsymbol{X}_2^{(0)},\cdots,\boldsymbol{X}_b^{(0)},\cdots,\boldsymbol{X}_B^{(0)}) \tag{90}$$

The dynamic adaptive Kalman filter-Gray model is used to model $\boldsymbol{X}_b^{(0)}$sequentially, obtaining the set of predicted measurement values $\hat{\boldsymbol{X}}$ at time k+1:

$$\hat{\boldsymbol{X}}=(\hat{x}_1^{(0)}(k+1),\hat{x}_2^{(0)}(k+1),\cdots,x_B^{(0)}(k+1)) \tag{91}$$

(3) The probability density function when the actual measured value k+1 is approximated by the above equation (91):

$$f_{k+1}=f(x) \tag{92}$$

where $f(\cdot)$ is the Gray self-help probability density function and x represents a measured variable value used to describe the measured value $\hat{x}_b^{(0)}(k+1)$during the dynamic measurement process.

(4) The measured value at sample point $k+1$ can be estimated using the mathematical expectation of set $\hat{\boldsymbol{X}}$ of the predicted measured values:

$$X_0=\hat{x}^{(0)}(k+1)=\int_{-\infty}^{+\infty}f(x)xdx \tag{93}$$

Rewriting the above expression into a discrete form:

$$X_0=\hat{x}^{(0)}(k+1)=\sum_{t=1}^{T}F(x_t)x_t \tag{94}$$

X_0 : Estimated true value; T:f_{k+1} is divided into T groups
x_t : Median value of the t group;
$F(\cdot)$: Probability distribution function of $\hat{X}$;

(3) Assuming the significant level is α, then in the case of confidence level $P=(1-\alpha)\times 100\%$, the measured value $\hat{x}^{(0)}(k+1)$ estimation interval can be defined as follows:

$$[X_L,X_U]=[X_{\alpha/2},X_{1-\alpha/2}] \tag{95}$$

$X_{\alpha/2}$: Estimated measurement value corresponding to confidence level $\alpha/2$ at sample point n+1;
X_L : Estimation interval lower bound;
X_U : Estimated interval upper bound;

(6) The dynamic expanded uncertainty of the dynamic adaptive Kalman filter-Gray bootstrap method at k+1 is defined as:

$$U=X_U-X_L \tag{96}$$

(7) K is added to the single step, the original measured value sequence is updated and steps (1)-(6) are repeated to evaluate the dynamic measurement uncertainty at the next sampling point. To make a more appropriate representation of the dynamic measurement uncertainty, the standard measurement uncertainty $u(k+1)$ at sample point $k+1$ is estimated from the standard deviation of the prediction set $\hat{X}$:

$$u(k+1)=\sqrt{\frac{\sum_{b=1}^{B}\left(x_b^{(0)}(n+1)-X_0\right)^2}{B-1}} \tag{97}$$

The uncertainty of the dynamic measurement for the entire measurement system can be assessed using the average measurement uncertainty:

$$U_{mean}=\sqrt{\frac{1}{N}\sum_{k=1}^{N}u^2(k)} \tag{98}$$

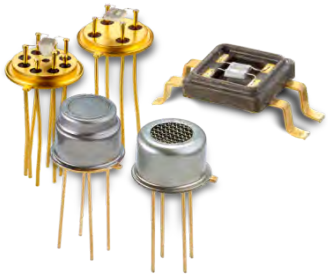

FIGURE 3. 3-array MOS gas sensor.

FIGURE 4. 3-array MOS gas sensor array signal acquisition board.

V. DYNAMIC MEASUREMENT UNCERTAINTY EVALUATION EXPERIMENT

To verify the validity of the proposed algorithms, this experiment uses 15 of the German UST company's 3-array MOS gas sensors to form a 45-array gas sensor. The 3-array MOS gas sensor is shown in Figure 3. Each 3-array MOS gas sensor array signal acquisition board is shown in Figure 4.

A. DYNAMIC ADAPTIVE KALMAN FILTER-GRAY PREDICTION PERFORMANCE COMPARISON EXPERIMENT

1) EXPERIMENTAL METHOD

Dynamic adaptive Kalman filter-Gray prediction contrast experiment. In this experiment, the 45-array MOS gas sensor is used as the experimental setup for the target gas, producing a normal response signal. It is then compared with the common Gray GM (1,1) prediction model, a BP neural network prediction model, and the RVM prediction model. The experimental method is as follows: historical data is used to model different prediction models in an online training mode and the prediction of the next sampling point of the sensor is realized in each sampling period. The prediction accuracy of the prediction model is evaluated by the following three commonly used evaluation indicators.

The Mean Absolute Percentage Error (MAPE) is a general method for estimating the accuracy of the predictions. It can represent the relative deviation between the measured values and predicted values. The formula is given in equation (99):

$$MAPE = \frac{1}{n}\sum_{k=1}^{n}\left|\frac{x^{(0)}(k) - \hat{x}^{(0)}(k)}{x^{(0)}(k)}\right| \times 100\% \qquad (99)$$

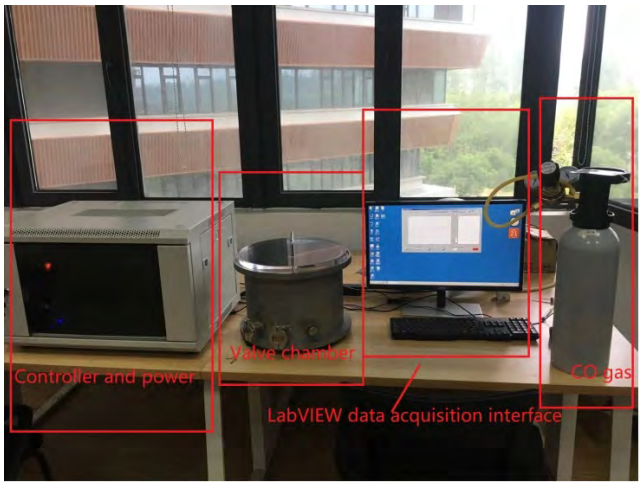

FIGURE 5. Static valve distribution laboratory equipment.

The Mean Squared Error (MSE) is an evaluation criterion for testing the average of the prediction errors:

$$MSE = \frac{1}{n}\sum_{k=1}^{n}(x^{(0)}(k) - \hat{x}^{(0)}(k))^2 \qquad (100)$$

The Absolute Mean Error (AME) is an evaluation criterion for testing the average of the prediction errors:

$$AME = \frac{1}{n}\sum_{k=1}^{n}|x^{(0)}(k) - \hat{x}^{(0)}(k)| \qquad (101)$$

The above three prediction model evaluation methods are used: MPAE, MSE, AME and prediction time are used to evaluate the prediction effects of the above four prediction models.

2) EXPERIMENTAL SAMPLE

As shown in Figure 5, the Static Valve Distribution Laboratory Equipment consists mainly of four parts: controller and power; valve chamber; LabVIEW data acquisition interface; and a gas source.

Taking CO as the experimental sample, the temperature of the air chamber was set to 20°C and relative humidity to 30%, The sensor array was placed in a 15 L measurement chamber, gas sensor was heated to 320°C, and the gas sample was injected statically with a syringe. The operating voltage of the sensors was kept constant at 5 V for the entire duration of the experiments. The sampling frequency of the sensor data continued at 5 Hz. The concentration of corresponding gas at different time periods is shown in Table 4.

3) EXPERIMENTAL RESULTS AND ANALYSIS

As shown in Figure 5, the MOS gas sensor actually measures the voltage value of the CO gas sensitive resistor. Using Figures 6 and 7, which show the LabVIEW data acquisition interface, 1200 sample resistance values can be obtained. The data is stored in the file in Fig. 6, the 1200 sample resistance

TABLE 4. Concentration of gas corresponding to different time periods.

Gas type	Times	Concentration
CO	0-80	400
CO	81-160	800
CO	161-240	1200

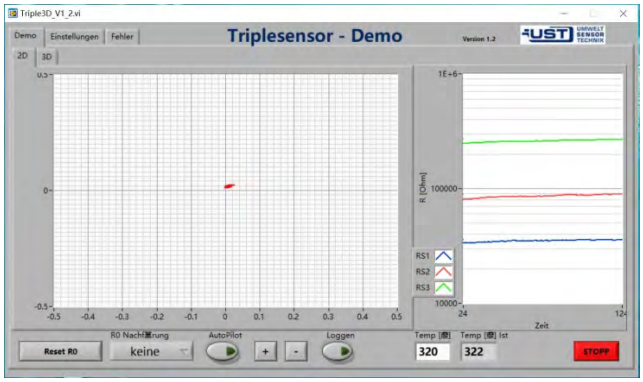

FIGURE 6. LabVIEW data acquisition interface.

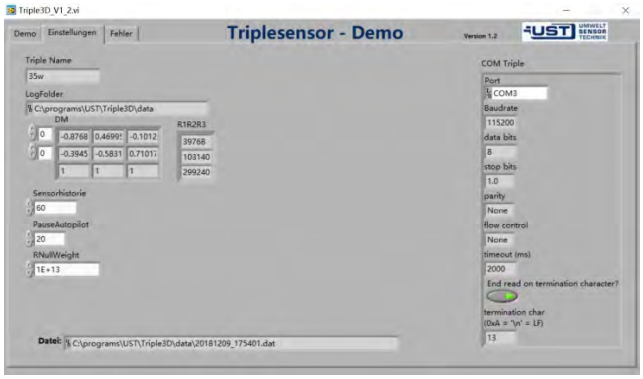

FIGURE 7. LabVIEW data storage interface.

values are calculated into the actual voltage value. The two-dimensional coordinate map of the voltage sample value and time relationship is shown in Figure 8.

Figure 9 shows the prediction results using the dynamic adaptive Kalman filter-Gray bootstrap comprehensive modified prediction model. To verify the feasibility and superiority of the algorithm, the data of the first 80 s are predicted in 2, 3, and 4 second interval. A total of 40 points are predicted. 57 points are predicted for 80 s∼160 s, 60 points are predicted for 160 s∼240 s, and the last three points are predicted beyond 240 s.

First, the known historical data are preprocessed, and the cumulative generating sequence $X^{(1)}$ is used to construct the Kalman filter model. After a Kalman filter calculation, the filtering value $X^{(n)}(n/n)$ of the $X^{(1)}$sequence is obtained. The GM (1,1) model is established by a cumulative sequence $X^{(0)}(k+1) = X^{(1)}(k+1/k+1) - X^{(1)}(k/k)$, and the parameters are obtained by a robust estimation in the process

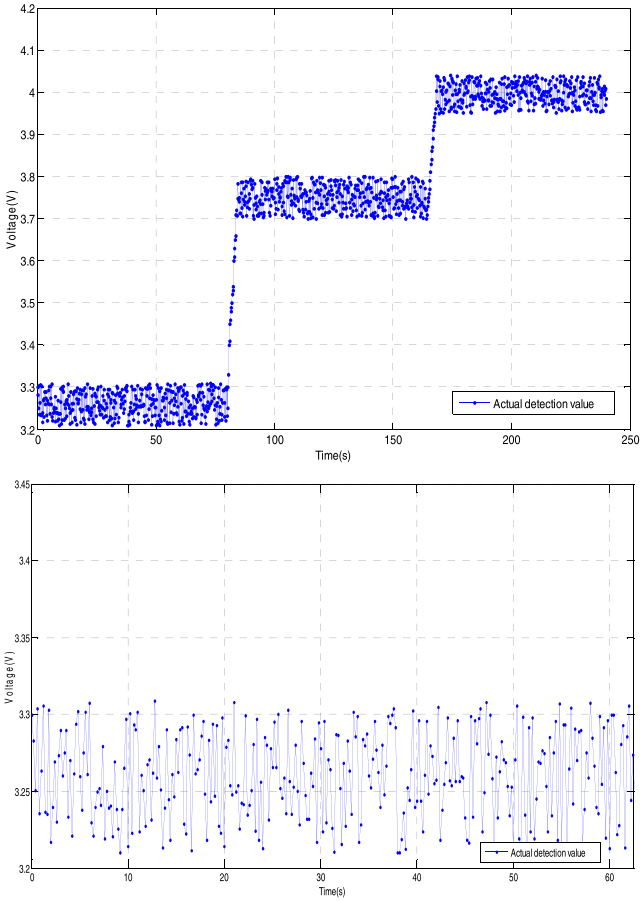

FIGURE 8. MOS gas sensor array detection of CO concentration value-time diagram.

of establishing the GM (1,1) model. According to the internal coincidence accuracy of the established model, the corresponding residual correction model for the residual sequence $\delta_M^{(0)}$ is established to modify the prediction model. According to the prediction equation of different spacing data series, multiple sets of predictive values $\hat{X}_{(t)}^{0}(k+1)$ are obtained. The final prediction result $\hat{X}^{(0)}(k+1)$ is synthesized by data fusion. The final prediction result $\hat{X}^{(0)}(k+1)$ is calculated according to the observed value L_{k+1}, and the variance component is calculated according to the residual. The dynamic noise estimate $\sigma_{\Omega_0}^2$ is obtained, and the filtering equation is optimized continuously by modifying the variance of the dynamic noise to overcome the instability of the filtering.

Figure 10 shows the BP neural network model prediction results. The number of neuron nodes in the input layer is set to 30, and the number of neuron nodes in the output layer is 3. At each point in time 30 measured values are known by historical measurement, 3 predicted values with intervals of 2, 3, and 4 seconds are predicted, and the number of selected nodes is continuously optimized by using a single-layer hidden layer network. This paper finally determines 10 nodes in the hidden layer, the activation function is selected as the tangent function, the initial = initial weight is set as the random number between (−1, 1), the initial value is selected

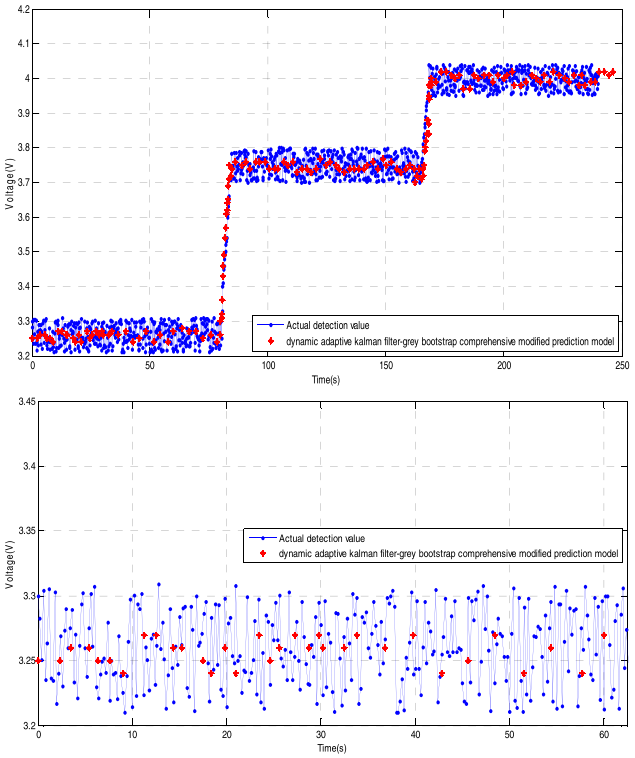

FIGURE 9. Dynamic adaptive Kalman filter-Gray bootstrap comprehensive modified prediction model results.

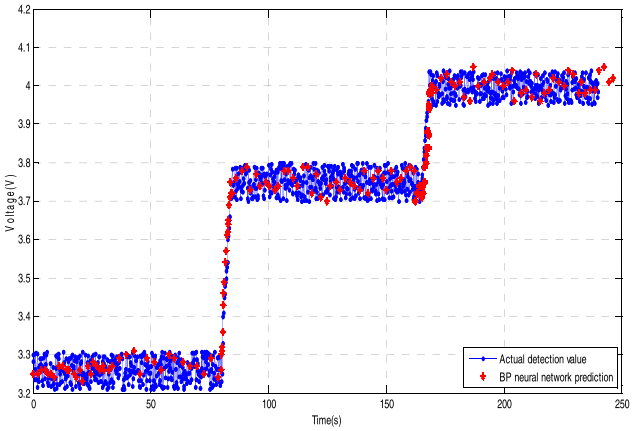

FIGURE 10. BP neural network model prediction results.

as the random number between (0, 1), the learning rate is set to 0.1, and the learning rate is initially set to 0.6, using the method of varying learning rate.

Figure 11 shows the results of the Gray GM (1,1) prediction model. From the sampled data, an estimated value is predicted by Gray theory for every interval of 2, 3, and 4 seconds. From 0 to 80 seconds, 40 estimated values are randomly predicted from the sampled 400 sample data. The same is done from 81 to 160 seconds. Of the sample data, 57 estimates were randomly predicted at 161-240 seconds, and 60 estimates were randomly predicted from the sampled

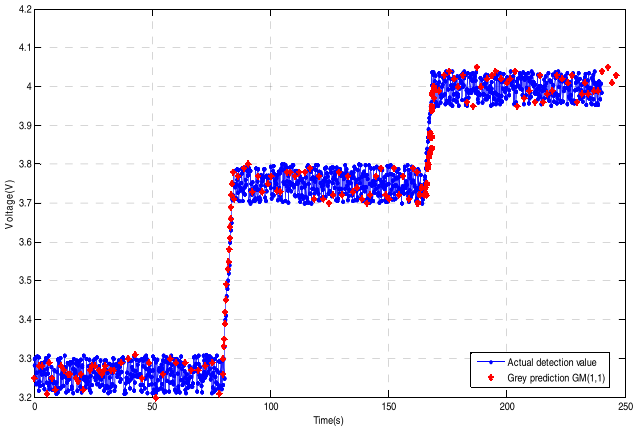

FIGURE 11. Gray GM (1,1) prediction model.

400 sample data. The last three points are predicted beyond 240 s.

The prediction model is as follows:

$$X = \{x(1, x(2), \cdots x(k), \cdots, x(n)\}(n = 10, 15, 20) \quad (102)$$

where x(k) is the measured value corresponding to sampling point k. To obtain the inherent law of the time series, the time series X0 is accumulated and generated to obtain a first-order cumulative generation sequence X1.

$$X^{(1)} = \{x^{(1)}(1), x^{(1)}(2), \cdots, x^{(1)}(k), \cdots, x^{(1)}(n)\} \quad (103)$$

$$x^{(1)}(k) = \sum_{i=1}^{k} x^{(0)}(i), \quad k = 1, 2, \cdots n \quad (104)$$

The basic form of the Gray prediction model GM (1,1) is called the Gray difference equation as follows:

$$\frac{dx^{(1)}(k)}{dk} + az^{(1)}(k) = b, \quad k = 2, 3, \cdots n \quad (105)$$

a and b are expressed as the development coefficient and control coefficient, respectively. $z^{(1)}(k)$ is defined as the background value as:

$$z^{(1)}(k) = \alpha x^{(1)}(k) + (1 - \alpha)x^{(1)}(k - 1) \quad (106)$$

α is the background value adjustment factor, $\alpha \in [0,1]$, and the Gray prediction in this paper uses a = 0.5. According to the definition of the derivative:

$$\frac{dx^{(1)}(k)}{dk} = \lim_{\Delta k \to 0} \frac{x^{(1)}(k + \Delta k) - x^{(1)}(k)}{\Delta k} \quad (107)$$

Let Δk be the unit interval, so the above formula is changed to:

$$\frac{dx^{(1)}(k)}{dk} = x^{(1)}(k + 1) - x^{(1)}(k) = x^{(0)}(k + 1) \quad (108)$$

Substituting equations (106) and (108) into equation (105):

$$x^{(0)}(k + 1) = a[-(\alpha x^{(1)}(k) + (1 - \alpha)x^{(1)}(k - 1))] + b \quad (109)$$

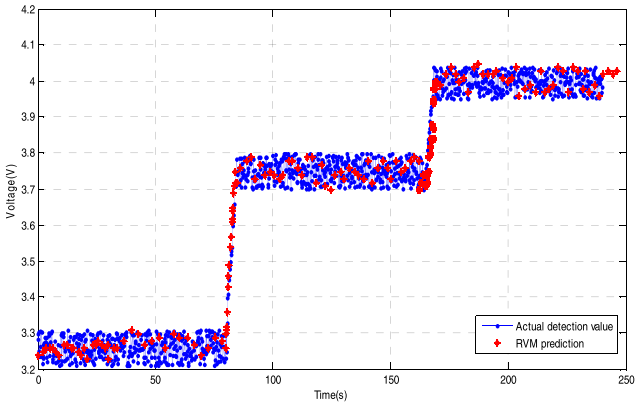

FIGURE 12. RVM model prediction results.

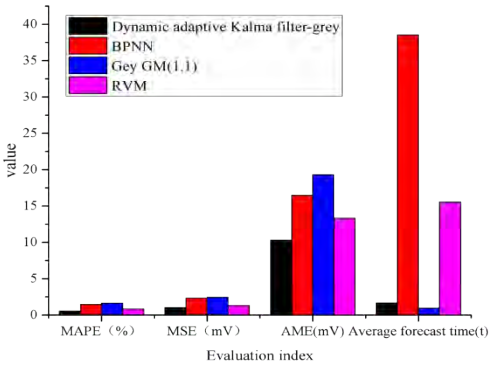

FIGURE 13. Prediction accuracy histogram of the four prediction models.

The parameters a and b to be determined can be obtained by the least squares method:

$$\hat{a} = [a, b]^T = (B^T B)^{-1} B^T Y$$
$$Y = \begin{pmatrix} x^{(0)}(2) \\ x^{(0)}(3) \\ \vdots \\ x^{(0)}(n) \end{pmatrix}, \quad B = \begin{pmatrix} -z^{(1)}(2) \\ -z^{(1)}(3) \\ \vdots \\ -z^{(1)}(n) \end{pmatrix} \tag{110}$$

The Gray prediction GM (1,1) time response function:

$$\hat{x}^{(1)}(k+1) = [x^{(1)}(1) - \frac{b}{a}]e^{-ak} + \frac{b}{a}$$
$$k = 2, 3, \cdots, 10/15/20 \tag{111}$$

The predicted value of the k+1 sampling point is calculated as follows:

$$\hat{x}^{(0)}(k+1) = \hat{x}^{(1)}(k+1) - \hat{x}^{(1)}(k)$$
$$= (1 - e^{a})[x^{(0)}(1) - \frac{b}{a}]e^{-ak}$$
$$k = 1, 2, 3, \cdots, 10/15/20 \tag{112}$$

Figure 12 shows the results of the RVM prediction. The data of the first 80 s are predicted by 2, 3, and 4 second intervals. A total of 40 points are predicted, 57 points are predicted for 80 s-160 s, 60 points are predicted for 160 s-240 s, and the last three points are predicted beyond 240 s.

The prediction model is as follows: the forecast output t^* is expressed as:

$$p(t^*|\mathbf{t}) = \int p(t^*|\mathbf{w}, \boldsymbol{\alpha}, \beta) p(\mathbf{w}, \boldsymbol{\alpha}, \beta|\mathbf{t}) d\omega d\alpha d\beta \tag{113}$$

This paper uses an iterative calculation to solve:

$$p(\mathbf{w}, \boldsymbol{\alpha}, \beta|t) = p(\mathbf{w}|\boldsymbol{\alpha}, \beta, t) p(\alpha, \beta|\mathbf{t}) \tag{114}$$

The posterior distribution of the weight vector $\boldsymbol{\omega}$ can be expressed as:

$$p(\boldsymbol{\omega}|\boldsymbol{\alpha}, \beta, \mathbf{t}) = \frac{p(\mathbf{t}|\mathbf{w}, \beta) p(\mathbf{w}|\boldsymbol{\alpha})}{p(\mathbf{t}|\boldsymbol{\alpha}, \beta)}$$
$$= (2\pi)^{-\frac{N+1}{2}} |\sum|^{-\frac{1}{2}}$$
$$\times \exp\{-\frac{(\mathbf{w} - \boldsymbol{\mu})^T \sum^{-1} (\mathbf{w} - \boldsymbol{\mu})}{2}\} \tag{115}$$

Posterior variance $\sum$ and mean μ are:

$$\sum = (\beta \boldsymbol{\Phi}^{\mathbf{T}} \boldsymbol{\Phi} + \mathbf{A})^{-1}$$
$$\boldsymbol{\mu} = \beta \sum \boldsymbol{\Phi}^{\mathbf{T}} \mathbf{t} \tag{116}$$

$\mathbf{A} = diag(a_0, a_1, \cdots, a_N)$, edge integration of weight w :

$$p(\mathbf{t}|\boldsymbol{\alpha}, \beta) = \int p(\mathbf{t}|\mathbf{w}, \beta) p(\mathbf{w}|\boldsymbol{\alpha}) dw \tag{117}$$

Ultra-parametric edge likelihood:

$$p(\mathbf{t}|\boldsymbol{\alpha}, \beta) = N(0, \mathbf{C})$$
$$\mathbf{C} = \beta^{-1}\mathbf{I} + \boldsymbol{\Phi}\mathbf{A}^{-1}\boldsymbol{\Phi}^{\mathbf{T}} \tag{118}$$

This paper uses an iterative method for an approximation. Superparameters a and b are expressed as:

$$\alpha_i^{new} = \frac{\gamma_i}{\mu_i^2}$$
$$\beta^{new} = \frac{N - \sum_i \gamma_i}{||y - \boldsymbol{\Phi}\mu||} \tag{119}$$

For sample data x^*, its predicted output y satisfies the Gaussian distribution:

$$p(y|\mathbf{t}) \sim N(\mu^T \boldsymbol{\Phi}(x^*), \beta^{-1}) \tag{120}$$

The mean $y = \mu^T \boldsymbol{\Phi}(x^*)$ is the predicted output of sample B of the RVM model in this paper.

The calculation formulas of the MAPE, MSE, and AME methods are shown in the formula above (99)-(101), and the prediction time is used as evaluation indicators to comprehensively evaluate the prediction effects of different prediction models. The evaluation results are shown in Figure 13. MAPE (%): dynamic adaptive Kalman filter-Gray bootstrap comprehensive modified prediction model 0.543, BP neural network (BPNN) 1.487, Gray GM (1,1) 1.632, RVM 0.832; MSE (mV): dynamic adaptive Kalman filter-Gray bootstrap comprehensive modified prediction model 0.123, BPNN 1.304, Gray GM (1,1) 0.691, RVM 0.627; AME (mV): dynamic adaptive Kalman filter-Gray bootstrap comprehensive modified prediction model 10.32, BPNN 16.523, Gray GM (1,1) 19.322, RVM 13.345; Average Forecast Time (ms): dynamic

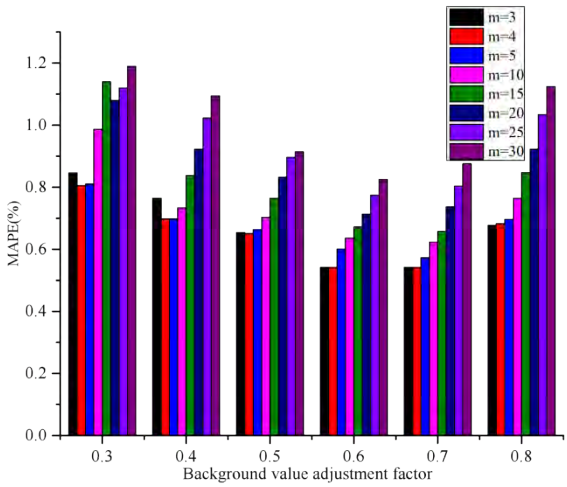

FIGURE 14. Average absolute percentage error with different parameters (%).

adaptive Kalman filter-Gray bootstrap comprehensive modified prediction model 1.65, BPNN 38.54,

Gray GM (1,1) 0.987, RVM 15.563; the BPNN has large values of MAPE, MSE and AME, a poor prediction performance and the longest average prediction time. The prediction performance of the RVM under small sample training conditions is smaller than that of the BP neural network and Gray GM (1,1). MAPE, MSE, and AME demonstrate better predictive performance but at the same time have a larger average forecast time.

The dynamic adaptive Kalman filter-Gray prediction ($m = 15, \alpha - = 0.6$) has the best prediction performance and the prediction time is longer than the Gray prediction model GM (1,1). It has obvious advantages over the BP neural network and RVM prediction model. Therefore, the dynamic adaptive Kalman filter-Gray prediction proposed in this paper can meet the real-time requirements, while obtaining a higher prediction accuracy.

The dynamic adaptive Kalman filter-Gray model proposed in this paper combines the GM (1,1), and its prediction accuracy is affected by the modeling length m and the background adjustment factor α. To obtain a suitable modeling length m and background value adjustment factor α, $\alpha = 0.3, 0.4, 0.5, 0.6, 0.7, 0.8$ and $m = 3, 4, 5, 10, 15, 20, 25, 30$, respectively, to establish different Dynamic adaptive Kalman filter-Gray model predictions of the measured value. MAPE is used as the evaluation index to obtain the MAPE histogram 11. As shown in Figure 14, it can be seen that the background value adjustment factor α obtains a higher prediction accuracy between 0.5-0.7, and the Gray modeling length m takes a reasonably small value to obtain a better prediction performance. The general background value adjustment factor α needs to select reasonable values according to different engineering applications. The background value adjustment factor of this paper takes $\alpha = 0.6$, and the growth of the Gray modeling length m may lead to a decrease in the prediction accuracy. The detailed proof process is given in paper [24]. Therefore, this paper uses $m = 15$.

4) EXPERIMENTAL CONCLUSION

The proposed dynamic adaptive Kalman filter-Gray prediction algorithm has a good prediction performance for an MOS gas sensor array application. Compared with other prediction algorithms, it has a short execution time and high prediction precision. It is especially suitable for dynamic signal pretesting under small sample and poor information conditions.

B. DYNAMIC ADAPTIVE KALMAN FILTER-GRAY BOOTSTRAP METHOD UNCERTAINTY EVALUATION EXPERIMENT

1) EXPERIMENTAL METHOD

A complete measurement dataset includes the measurement value and the measurement uncertainty composition. Especially in the dynamic measurement process, the uncertainty reflects the accuracy of obtaining the measured value. The MOS gas sensor array measurement system is a typical dynamic measurement system, and the determination of the uncertainty source is difficult. Experimental principle: set the dynamic adaptive Kalman filter-Gray bootstrap method modeling length $m = 15$, resampling times $B = 2500$, background value adjustment factor α and confidence level $p = 97.5\%$. The uncertainty of the MOS gas sensor array is evaluated. The purpose of the experiment is to validate the dynamic adaptive Kalman filter-Gray self-help method for an uncertainty evaluation using real MOS gas sensor experimental samples.

2) EXPERIMENTAL SAMPLE

Taking CO as the experimental sample, in the temperature range: 20°C C, relative humidity: 30%, during the first 80 s, the CO gas concentration is 400 ppm, between 80-160 s the CO gas concentration is 800 ppm and between 160-240 s the CO gas concentration is 1200 ppm. The MOS gas sensor response signal of each stage was acquired experimentally.

3) EXPERIMENTAL RESULTS

Using the introduction in ćô Uncertainty Evaluation Algorithm In Dynamic Measurement State, calculate X_L and X_U by using equations (89)-(95). Bring the predicted value of the above dynamic adaptive Kalman filter-Gray comprehensive correction prediction model into equation (91). As shown in the experimental results of Figures 15 and 16, the confidence interval obtained by the dynamic adaptive Kalman filter-Gray Bootstrap method can envelope the measured signal value of the MOS gas sensor array. The dynamic measurement uncertainty of the MOS gas sensor array estimated by the dynamic adaptive Kalman filter-Gray Bootstrap method is shown in Figure 17, and can be calculated by equation (96). The average uncertainty of the entire dynamic measurement process is calculated by the following formula (102):

$$U_{mean} = \sqrt{\frac{1}{N}\sum_{k=1}^{N} u^2(k)} = 0.041 \tag{121}$$

Therefore, the dynamic adaptive Kalman filter-Gray bootstrap comprehensive modified prediction model proposed in

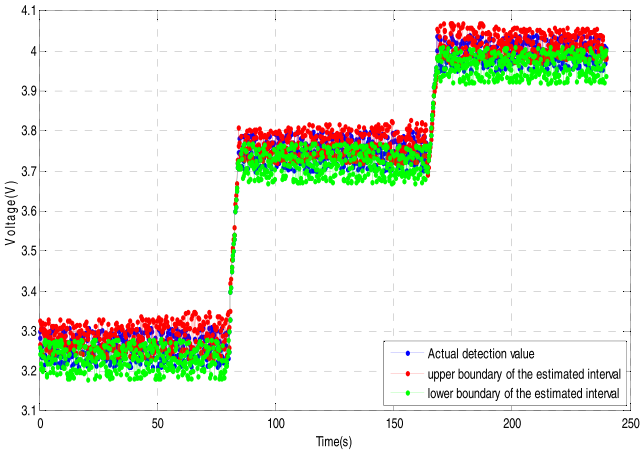

FIGURE 15. MOS gas sensor array detection signal and confidence interval diagram.

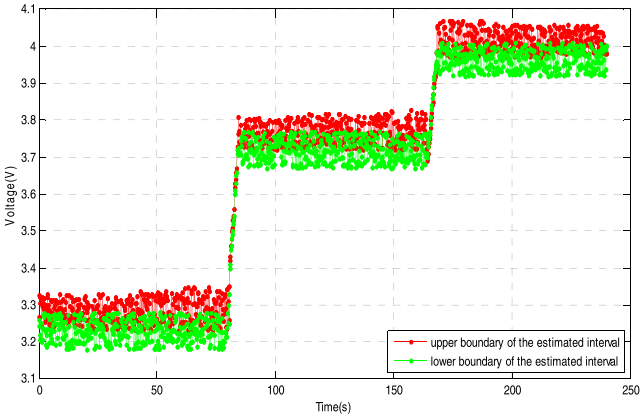

FIGURE 16. Confidence interval.

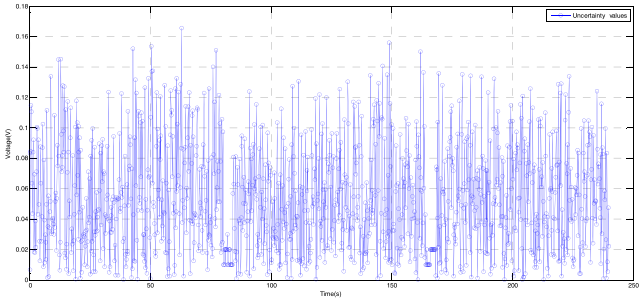

FIGURE 17. Uncertainty values in the dynamic measurement state of MOS gas sensor array.

this paper can enable the evaluation of the uncertainty of an MOS gas sensor array without prior knowledge of the uncertainty source and its probability distribution.

VI. CONCLUSION

In this paper, based on the evaluation of the dynamic measurement uncertainty of MOS gas sensor arrays, a dynamic adaptive Kalman filter-Gray bootstrap comprehensive modified prediction model for uncertainty evaluation is proposed. The dynamic adaptive Kalman filter-Gray bootstrap method is used to measure the probability distribution function. Through an effective estimation, the uncertainty evaluation of the dynamic measurement state of the MOS gas sensor array is realized through experiments and the reliability of the evaluation result is improved. To improve the accuracy of the measurement value, which is being reduced due to partial failure of the MOS gas sensor array, sensor dynamics are utilized. Using an adaptive Kalman Filter-Gray Prediction Model Correlation of the multisensor output, an XOR MOS gas sensor array measurement value confirmation algorithm is proposed to accurately distinguish the measured value of the measured gas from the normal dynamic abrupt change. Finally, the MOS gas sensor array experimental platform is built to verify the dynamic measurement uncertainty evaluation algorithm, proving that the proposed two algorithms represent an improvement over current state of the art algorithms.

REFERENCES

[1] C. De Capua and E. Romeo, "A smart THD meter performing an original uncertainty evaluation procedure," *IEEE Trans. Instrum. Meas.*, vol. 56, no. 4, pp. 1257–1264, Aug. 2007.

[2] M. Pertile, M. De Cecco, and L. Baglivo, "Uncertainty evaluation in two-dimensional indirect measurement by evidence and probability theories," *IEEE Trans. Instrum. Meas.*, vol. 59, no. 11, pp. 2816–2824, Nov. 2010.

[3] S. A. Farooqui, T. Doiron, and C. Sahay, "Uncertainty analysis of cylindricity measurements using bootstrap method," *Measurement*, vol. 42, no. 4, pp. 524–531, May 2009.

[4] Z. Shen and Q. Wang, "Data validation and validated uncertainty estimation of multifunctional self-validating sensors," *IEEE Trans. Instrum. Meas.*, vol. 62, no. 7, pp. 2082–2092, Jul. 2013.

[5] Y. Chen, S. Jiang, J. Yang, K. Song, and Q. Wang, "Grey bootstrap method for data validation and dynamic uncertainty estimation of self-validating multifunctional sensors," *Chemometrics Intell. Lab. Syst.*, vol. 146, pp. 63–76, Aug. 2015.

[6] L. Peretto, R. Sasdelli, and R. Tinarelli, "On uncertainty in wavelet-based signal analysis," *IEEE Trans. Instrum. Meas.*, vol. 54, no. 4, pp. 1593–1599, Aug. 2005.

[7] Z. Shen and Q. Wang, "Failure detection, isolation, and recovery of multifunctional self-validating sensor," *IEEE Trans. Instrum. Meas.*, vol. 61, no. 12, pp. 3351–3362, Dec. 2012.

[8] Y. Chen, J. Yang, Y. Xu, S. Jiang, X. Liu, and Q. Wang, "Status self-validation of sensor arrays using gray forecasting model and bootstrap method," *IEEE Trans. Instrum. Meas.*, vol. 65, no. 7, pp. 1626–1640, Jul. 2016.

[9] A. He, G. Wei, J. Yu, Z. Tang, Z. Lin, and P. Wang, "A novel dictionary learning method for gas identification with a gas sensor array," *IEEE Trans. Ind. Appl.*, vol. 64, no. 12, pp. 9709–9715, Dec. 2017.

[10] L. Zhang and D. Zhang, "Domain adaptation extreme learning machines for drift compensation in E-nose systems," *IEEE Trans. Instrum. Meas.*, vol. 64, no. 7, pp. 1790–1801, Jul. 2015.

[11] J. Yu, J. Li, Q. Dai, D. Li, X. Ma, and Y. Lv, "Temperature compensation and data fusion based on a multifunctional gas detector," *IEEE Trans. Instrum. Meas.*, vol. 64, no. 1, pp. 204–211, Jan. 2015.

[12] C. Massie, G. Stewart, G. McGregor, and J. R. Gilchrist, "Design of a portable optical sensor for methane gas detection," *Sens. Actuators B, Chem.*, vol. 113, no. 2, pp. 830–836, Feb. 2006.

[13] H. Yu, P. Xu, X. Xia, D.-W. Lee, and X. Li, "Micro-/nanocombined gas sensors with functionalized mesoporous thin film self-assembled in batches onto resonant cantilevers," *IEEE Trans. Ind. Electron.*, vol. 59, no. 12, pp. 4881–4887, Dec. 2012.

[14] F. Bertocci *et al.*, "Assessment and optimization for novel gas materials through the evaluation of mixed response surface models," *IEEE Trans. Instrum. Meas.*, vol. 64, no. 4, pp. 1084–1092, Apr. 2015.

[15] K. Yhland and J. Stenarson, "Measurement uncertainty in power splitter effective source match," *IEEE Trans. Instrum. Meas.*, vol. 56, no. 2, pp. 669–672, Apr. 2007.

[16] L. Angrisani, R. S. L. Moriello, and M. D'Apuzzo, "New proposal for uncertainty evaluation in indirect measurements," *IEEE Trans. Instrum. Meas.*, vol. 55, no. 4, pp. 1059–1064, Aug. 2006.
[17] A. Ferrero and S. Salicone, "Fully comprehensive mathematical approach to the expression of uncertainty in measurement," *IEEE Trans. Instrum. Meas.*, vol. 55, no. 3, pp. 706–712, Jun. 2006.
[18] L. Angrisani, M. D'Apuzzo, and R. S. L. Moriello, "Unscented transform: A powerful tool for measurement uncertainty evaluation," *IEEE Trans. Instrum. Meas.*, vol. 55, no. 3, pp. 737–743, Jun. 2006.
[19] D. A. Lampasi, F. Di Nicola, and L. Podesta, "Generalized lambda distribution for the expression of measurement uncertainty," *IEEE Trans. Instrum. Meas.*, vol. 55, no. 4, pp. 1281–1287, Aug. 2006.
[20] D. A. Lampasi, "An alternative approach to measurement based on quantile functions," *Measurement*, vol. 41, no. 9, pp. 994–1013, Nov. 2008.
[21] C. H. Sim and M. H. Lim, "Evaluating expanded uncertainty in measurement with a fitted distribution," *Metrologia*, vol. 45, no. 2, p. 178, 2008.
[22] L. Angrisani, M. D'Apuzzo, R. Schiano, and L. Moriello, "New proposal for uncertainty estimation in indirect measurements with correlated input quantities," *IEEE Trans. Instrum. Meas.*, vol. 55, no. 4, pp. 2124–2129, Aug. 2006.
[23] F. Attivissimo, A. Cataldo, N. Giaquinto, and M. Savino, "Assessment of the uncertainty associated with systematic errors in digital instruments: An experimental study on offset errors," *Meas. Sci. Technol.*, vol. 23, no. 3, 2012, Art. no. 035004.
[24] L. Wu, S. Liu, L. Yao, and S. Yan, "The effect of sample size on the grey system model," *Appl. Math. Model.*, vol. 37, no. 6, pp. 6577–6583, 2013.

WENWEN ZHANG received the M.S. degree in control science and engineering from the University of Shanghai for Science and Technology, Shanghai, China, in 2017. He is currently pursuing the Ph.D. degree in control science and engineering with Tongji University, China.

His current research interests include machine olfactory, sensor detection technology, sensor fault diagnosis, multisensory data fusion, and intelligent testing.

LEI WANG received the B.S. degree in automation and the M.S. degree in control science and engineering from Northwestern Polytechnical University, Xi'an, China, in 1982 and 1985, respectively, and the Ph.D. degree from Duisburg-Essen University, Duisburg, Germany.

He is currently a lifetime Professor with the Sino-German Institute, Tongji University. His current research interests include sensor detection technology and sensor fault diagnosis, multisensory data fusion, intelligent testing, and unmanned aerial vehicle (UAV) reverse technology.

LIHUA YE received the B.S. degree in electrical engineering from Dalian Railway University, Dalian, China, in 2000, and the M.S. degree in automation from Southwest Jiaotong University. He is currently pursuing the Ph.D. degree in control science and engineering with Tongji University, China.

He is also a Lecturer with the Department of Mathematical and Information Engineering, Jiaxing University. His current research interests include machine learning and computer vision, sensor detection technology and sensor fault diagnosis multisensory data fusion, and intelligent testing.

PEILONG LI received the B.S. degree in automation form the Taiyuan University of Technology, Taiyuan, China, in 2008, and the M.S. degree in control science and engineering from Tongji University, Shanghai, China, in 2012, where he is currently pursuing the Ph.D. degree in control science and engineering.

His current research interests include sensor detection technology and sensor fault diagnosis, multisensory data fusion, and intelligent testing.

MINGXUE HU received the B.S. degree in automation from the Nanjing University of Posts and Telecommunications, Nanjing, China, in 2017. She is currently pursuing the M.S. degree in control science and engineering with Tongji University.

Her current research interests include machine olfactory, sensor detection technology, sensor fault diagnosis, multisensory data fusion, and intelligent testing.